Polym. Bull. (2010) 64:115–126
DOI 10.1007/s00289-009-0135-y

Preparation and structural properties of Fe_3O_4–polyimide hybrid nanocomposites

Turgay Seckin · Sema Vural · Süleyman Köytepe

Received: 27 January 2009 / Revised: 28 April 2009 / Accepted: 8 July 2009 /
Published online: 26 July 2009

Abstract Polyimide films in which magnetic Fe_3O_4 nanoparticles are uniformly distributed are prepared. Before the preparation of the Fe_3O_4–polyimide composites, pure magnetite nanoparticles (Fe_3O_4) have been synthesized in water by co-precipitation (from ferric chlorides). Its surface was firstly modified with the 3-aminopropyl triethoxysilane. The prepared polyimide–Fe_3O_4 nanocomposite films were characterized for their structure, morphology, and thermal behavior employing Fourier transform infrared spectroscopy, scanning electron micrograph, X-ray diffraction, and thermal analysis (DTA/TGA/DSC) techniques.

Keywords Polyimides · Nanoparticles · Nanomaterial · Magnetics · Magnetic material · Sol-gel

Introduction

Among the heat resistant and high performance polymers, polyimides have received considerable scientific and technological attention due to their outstanding performance such as dielectrical and mechanical properties, thermal and chemical stability [1–7]. The applications of polyimides range from aerospace to microelectronics to medical, largely due to the fact that they offer certain desirable properties. Several potential applications of polyimides have appeared in the literature for advanced technology such as internal dielectric photoresist, membrane, photoconductor, light emitting diode and nonlinear optical materials. Further interest in their functional construction and application has been increasing in order to obtain polyimides possessing certain specific properties [7–21].

T. Seckin (✉) · S. Vural · S. Köytepe
Chemistry Department, İnonu University, 44280 Malatya, Turkey
e-mail: tseckin@inonu.edu.tr

Recently, conducting polymer nanocomposites with both electrical and ferromagnetic properties have generated tremendous attraction, and they have become one of the most active and promising research areas [22–27]. These materials are largely being used in nonlinear optics, electrochemical display devices, molecular electronics, electrical and magnetic shields and microwave absorbing materials. The large surface to volume ratio of the nanoparticles results in the formation of composites with unusual physical and chemical properties.

In this study, novel Fe_3O_4–polyimide hybrid nanocomposite were prepared by imidization and blending the required ratios of 3-aminopropyl triethoxysilane (APTS)-coated Fe_3O_4 nanoparticle and various dianhydride using *N*-methyl-2-pyrrolidone (NMP) as aprotic solvent. Since it has long been known that Fe_3O_4 exhibits excellent magnetic property, the prepared polyimide–Fe_3O_4 nanocomposite films were characterized for their structure, morphology, and thermal behavior employing Fourier transform infrared spectroscopy (FTIR), scanning electron micrograph (SEM), X-ray diffraction (XRD), and thermal analysis (DTA/TGA/DSC) techniques. These studies showed the homogenous dispersion of Fe_3O_4 in the polyimide matrix.

Experimental section

Materials

All chemicals were purchased form Aldrich and used after purification. NMP was distilled over CaH_2 under reduced pressure and stored over 4 Å molecular sieves. Reagent grade aromatic dianhydrides such as pyromellitic dianhydride (PMDA), 3,3′,4,4′-benzophenonetetracarboxylic dianhyride (BPDA), 4,4′-oxydiphthalic anhydride (ODPA) that was sublimed at 250 °C under reduced pressure, 3,3′,4,4′-biphenyltetracarboxylic dianhydride (BTDA) was used after crystallization in proper solvents. All the dianhydrides were dried under vacuum at 120 °C prior to use.

Instrumentation

The samples were characterized by XRD for the crystal structure, average particle size and the concentration of impurity compounds present. Rigaku Rad B-Dmax II powder X-ray diffractometer was used for XRD patterns of these samples. The 2θ values were taken from 20°–110° with a step size of 0.04° using Cu Kα radiation (λ value of 2.2897 Å). The dried samples were dusted on to plates with low background. A small quantity of 30($\pm$2) mg spread over 5 cm^2 area used to minimize error in peak location and also the broadening of peaks due to thickness of the sample is reduced. This data illustrate the crystal structure of the particles and also provides the inter-planar space, d. The broadening of the peak was related to the average diameter (L) of the particle according to Scherrer's formula, i.e. $L = 0.9\lambda/\Delta \cos\theta$ where λ is X-ray wavelength, Δ is line broadening measured at half-height and θ is Bragg angle of the particles.

Infrared spectra were recorded as KBr pellets in the range 4,000–400 cm^{-1} on an ATI UNICAM systems 2000 Fourier transform spectrometer. Differential scanning calorimetry (DSC), differential thermal analysis (DTA) and thermogravimetry (TG) were performed with Shimadzu DSC-60, DTA-50 and TGA-50 thermal analyzers, respectively.

Chemical composition analysis by EDAX was performed with an EDAX; Rönteck xflash detector analyzer associated to a scanning electron microscope (SEM, Leo-Evo 40xVP). Incident electron beam energies from 3 to 30 keV had been used. In all cases, the beam was at normal incidence to the sample surface and the measurement time was 100 s. All the EDAX spectra were corrected by using the ZAF correction, which takes into account the influence of the matrix material on the obtained spectra.

Procedures

Preparation of Fe_3O_4 nanoparticle

Fe_3O_4 nanoparticle was prepared by the conventional coprecipitation method. Firstly, 5.2 g of $FeCl_3$, 2.0 g of $FeCl_2$ and 0.85 mL of 12 mol/L HCl were dissolved in 25 mL of DI water under N_2 protection. And then the resulting solution was added drop-wise into 250 mL of 1.5 mol/L NaOH solution under vigorous stirring. After the reaction, the obtained precipitate was separated from the reaction medium under the magnetic field and washed with DI water for three times and ethanol for two times. Finally, a portion of Fe_3O_4 nanoparticles was dispersed in ethanol with the concentration of 5 g/L

APTS-coated Fe_3O_4 nanoparticle

The modification of Fe_3O_4 nanoparticles with APTS was performed in ethanol solution at room temperature and a small amount of water was added to accelerate to its hydrolysis. Typically, 25 mL of the above ethanol solution with 5 g/L of Fe_3O_4 nanoparticles was diluted to 150 mL with ethanol and 1 mL of H_2O. In order to disperse Fe_3O_4 nanoparticle well, the solution was further treated by ultrasonic wave for 30 min. After that, 0.4 mL of APTS was added with rapid stirring, and then the reactant mixture was stirred for another 7 h. Finally, the APTS-coated Fe_3O_4 nanoparticles were separated from the mixture by the ultracentrifugation and washed with ethanol for five times. Before the next step, the APTS-coated Fe_3O_4 nanoparticles were dispersed in ethanol with the concentration of 1 g/L.

Procedure for the determination of the amino content

The content of amino groups of the APTS-coated Fe_3O_4 nanoparticle was determined by consumption of HCl aqueous solutions. In a typical procedure, a 100 mL flask was charged with 0.10 g of APTS-coated Fe_3O_4 nanoparticle and 20 mL of 0.01 mol/L HCl aqueous solution, and the mixture was stirred at room temperature for 2 days, filtrated, and the filtrate was back titrated with NaOH (aq)

using an indicator. Then the amount of terminal amino groups per 1.0 g of APTS-coated Fe_3O_4 nanoparticle was calculated to be 12.2%.

Synthesis of the Fe_3O_4–PI nanocomposites

The polyimide–Fe_3O_4 hybrids were prepared by imidization and blending the required ratios of APTS-coated Fe_3O_4 nanoparticle and various dianhydride in NMP (Scheme 1) A typical polyimide synthesis was performed as follows: APTS-coated Fe_3O_4 nanoparticle (0.5 mmol) was dissolved in NMP (25 mL) in a 50 mL Schlenck tube equipped with a nitrogen line, overhead stirrer, a xylene-filled Dean-Stark trap, and a condenser. Dianhyride (4 mmol) in 5 mL of NMP was added to the amine solution and stirred overnight to give a viscous solution under nitrogen. The water, forming during the imidization process, can be removed from reaction mixture by the Dean-Stark trap and xylene. The mixture is heated to 70 °C, xylene (5 mL) was added and the mixture was refluxed for 3 h. During the reaction, the water is collected in the Dean-Stark trap. It followed by the removal of xylene by distillation. The mixture was transferred into an aluminum container and heated in a furnace under nitrogen atmosphere up to 130 °C at a ramp rate of 5 °C/min and kept at that temperature for 2 h. Then the sample was placed in a quartz tube and heated to several curing temperatures (100, 200, 300 and 400 °C) at a ramp rate of 5 °C/min and kept at this temperature for 4 h. The dark brown product was precipitated and dried at 100 °C under vacuum and then at 200–250 °C under nitrogen for 2 h; yield, 89%.

Results and discussion

Monomer characterization

For Fe_3O_4 nanoparticles dispersed in a neutral aqueous solution, the bare atoms of Fe and O on the particle surface would adsorb OH^- and H^+, respectively. As a result, there are many OH groups around the surface of Fe_3O_4 nanoparticles. In addition, because the reaction between OH on the surface and APTS can easily take place, APTS is usually employed to modify the surface of metal oxide. Figure 1 shows FTIR spectrum of APTS-coated Fe_3O_4 nanoparticles. This figure shows the presence of aliphatic stretching frequencies at 2,850–2,890 cm^{-1} in FTIR spectrum of APTS-coated Fe_3O_4. These stretching frequencies were not observed indicating the pure Fe_3O_4 nanoparticles. In Fig. 1 the peak at $\sim$3,439.4 cm^{-1} is attributed to the stretching vibrations of –OH, which is assigned to OH– absorbed by Fe_3O_4 nanoparticles and the peak at $\sim$600 cm^{-1} is attributed to the Fe–O bond vibration of Fe_3O_4 in both of the FTIR spectrum of APTS-coated Fe_3O_4 and Fe_3O_4 nanoparticles. In comparison with the standard spectra, following absorption bands can be observed: bands at 2,926.8 and 2,853.8 cm^{-1} due to the stretching vibration of C–H bond, band at 1,014.7 cm^{-1} due to the stretching vibration of Si–O bond, band at 1,091.1 cm^{-1} due to the stretching vibration of C–N bond and band at 885.2 cm^{-1} due to the bending vibration of NH_2 bond.

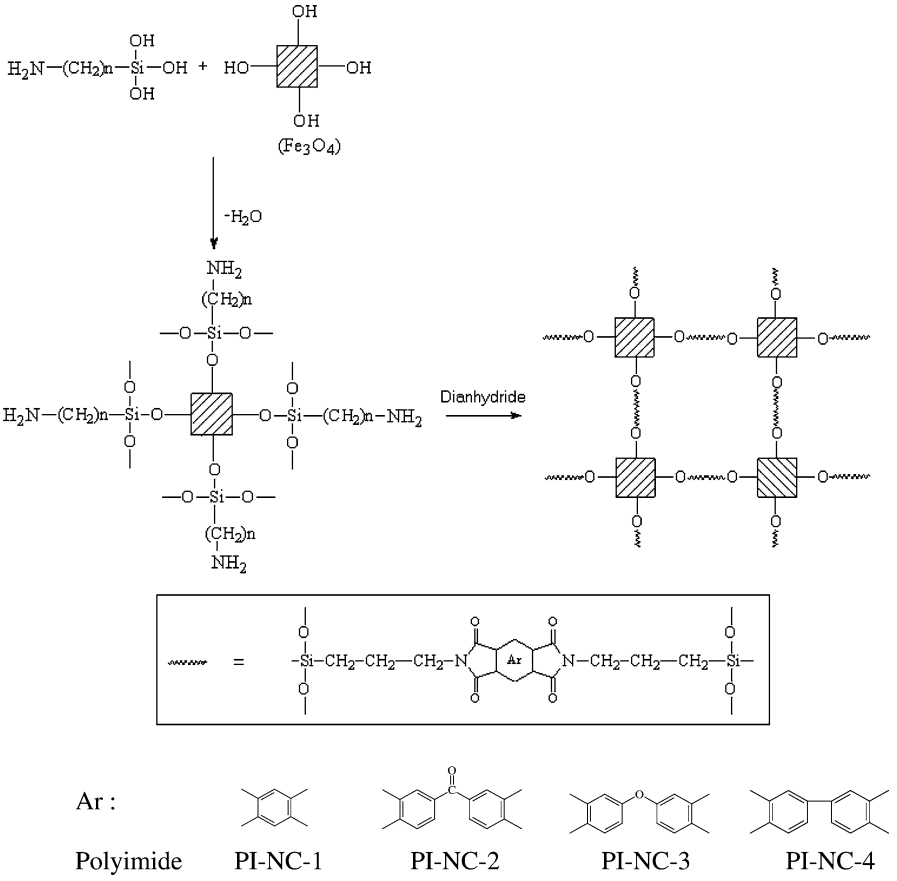

Scheme 1 Synthesis of PI–Fe $_3O_4$ nanocomposites

Moreover, the absorption bands at 3,416.5 and 1,629.5 cm^{-1} could be attributed to the co-contribution of NH_2 bond and remainder water in the sample. All of those bands reveal that the surface of Fe_3O_4 nanoparticles is successfully modified with APTS. Representative TEM image of APTS-coated Fe_3O_4 nanoparticles is shown in Fig. 2, from which it can be seen that most of the particles are quasi-spherical with an average diameter of 80 nm.

Differential thermal analysis and TGA curves of APTS-coated Fe_3O_4 and Fe_3O_4 nanoparticles were demonstrated in Fig. 3. TGA curves of the Fe_3O_4 and APTS-coated Fe_3O_4 composite particles (Fig. 3). Both particles showed H_2O loss of approximately 2% up to 100 °C. For Fe_3O_4 particles, a 1.8% weight decrease between 100 and 800 °C is probably related to further water loss and dehydroxylation. For organosilane-functionalized Fe_3O_4 composite particles, a 9.2% weight decrease between 100 and 800 °C is probably related to further water loss, dehydroxylation, and organic group decomposition. TGA analysis (Fig. 3a) shows that there was an increase in the organic content when Fe_3O_4 nanoparticles were

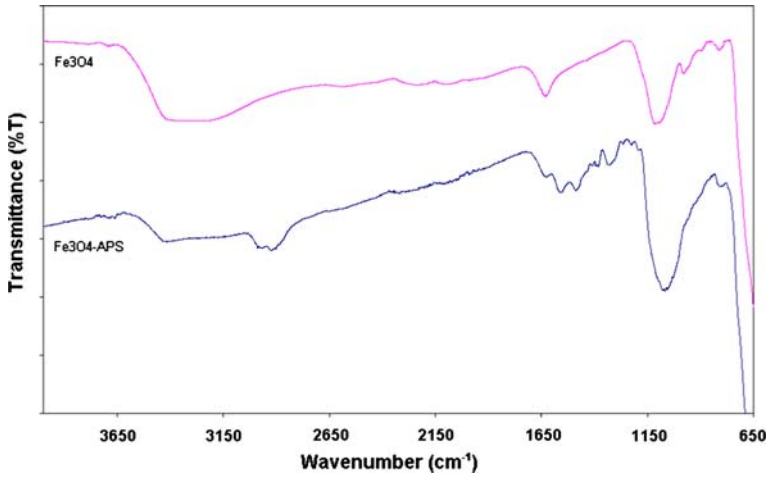

Fig. 1 FTIR spectrum of APTS-coated Fe_3O_4 and Fe_3O_4 nanoparticles

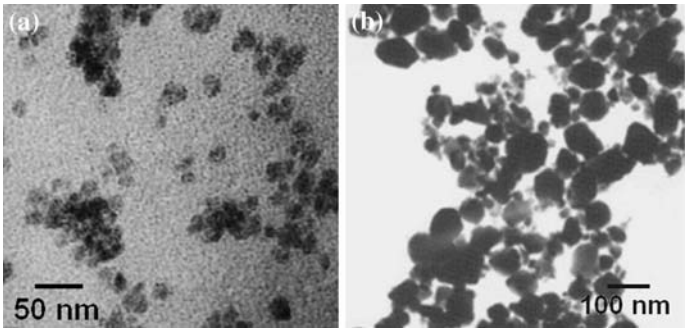

Fig. 2 TEM image of Fe_3O_4 nanoparticles (**a**) and APTS-coated Fe_3O_4 (**b**)

coated with APTS. The APTS-coated Fe_3O_4 contained 5.4% of organic material which belongs to APTS on the magnetite nanoparticles. This result is in good agreement with that of the DTA curves of the of APTS-coated Fe_3O_4 and Fe_3O_4 nanoparticles (Fig. 3b). For APTS-coated Fe_3O_4 composite particles, a band between 200 and 400 °C is probably related to organic group decomposition.

Characterization of the PI–Fe_3O_4 nanocomposites

PI–Fe_3O_4 nanocomposites (PI-NC-1–4) were synthesized by two-stage polycondensation of dianhydrides with APTS-coated Fe_3O_4 nanoparticles. All the polymerizations proceeded in homogeneous solution and the precipitation was prevented in all cases by adjusting the solvent to the monomer ratio. The FTIR spectrum of the PI–Fe_3O_4 nanocomposites is shown in Fig. 4. The FTIR spectra (Fig. 4) showed that aliphatic C–H stretching frequencies were appeared between 2,850 and 2,890 cm^{-1}, 1,720–1,730 cm^{-1} sym. imide ν (C=O), 1,765–1,790 cm^{-1}

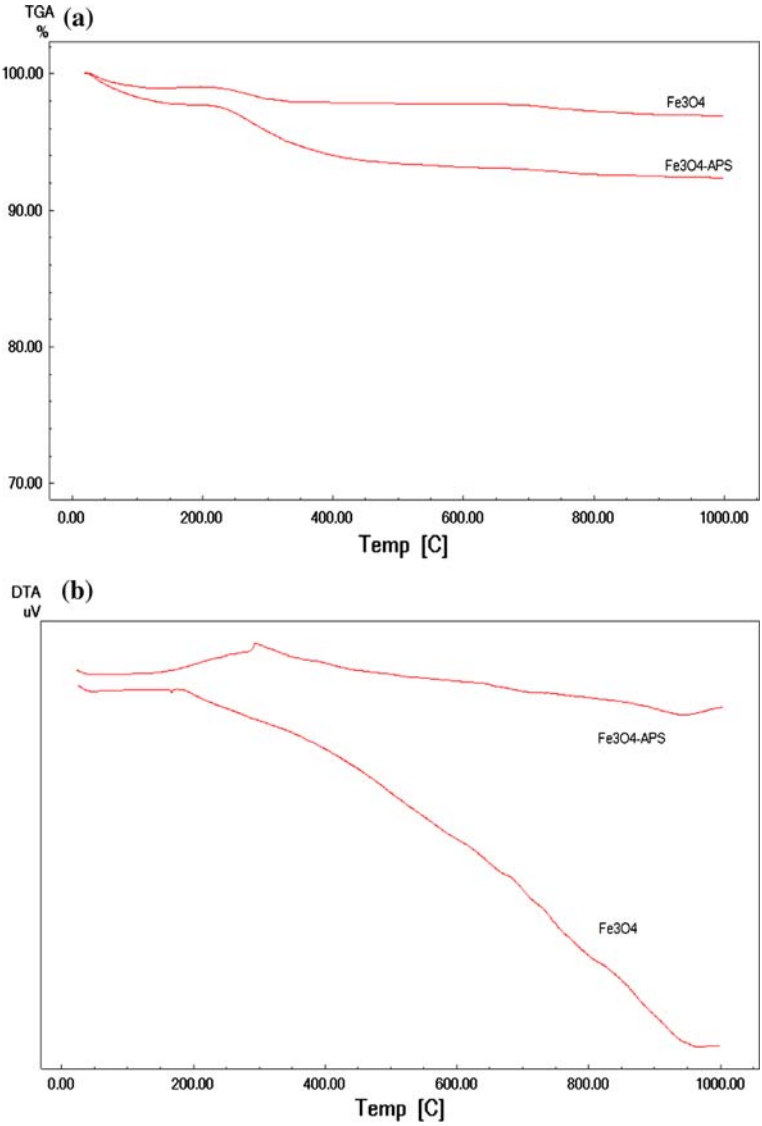

Fig. 3 TGA (**a**) and DTA (**b**) curves of APTS-coated Fe_3O_4 and Fe_3O_4 nanoparticles

asym. imide *v* (C=O) stretching, C–N imide ring stretching 1,360 cm^{-1}, whereas imide ring deformation was appeared at near 1,070 cm^{-1} and C–N bending at 730–760 $cm^{-1}$and the Si–O band in the monomers gave at 1,090 cm^{-1}, respectively [21].

The thermal properties of the polyimides were evaluated by DSC, DTA (Fig. 5) and TG (Fig. 6). DSC (Fig. 7) experiments were conducted at a heating rate of 10 °C/min in nitrogen. Rapid cooling from 400 °C to room temperature produced predominantly amorphous samples, so T_g's of all the polyimides could easily be

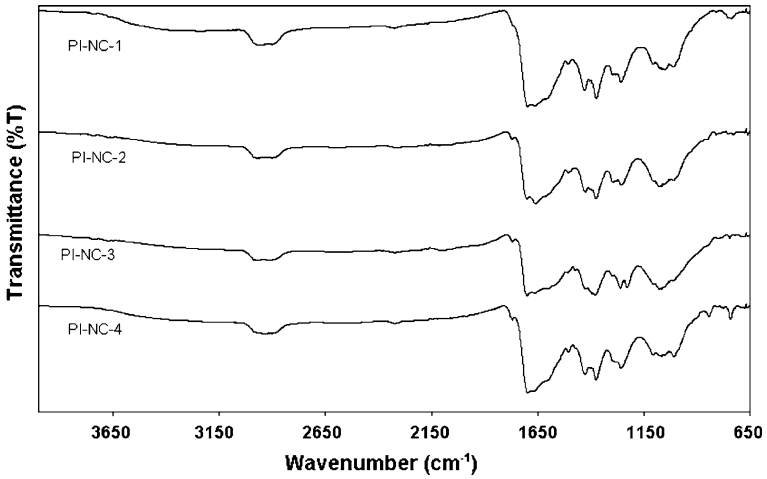

Fig. 4 FTIR Spectrum of polyimides prepared from APTS-coated Fe_3O_4 nanoparticles and various dianhydrides

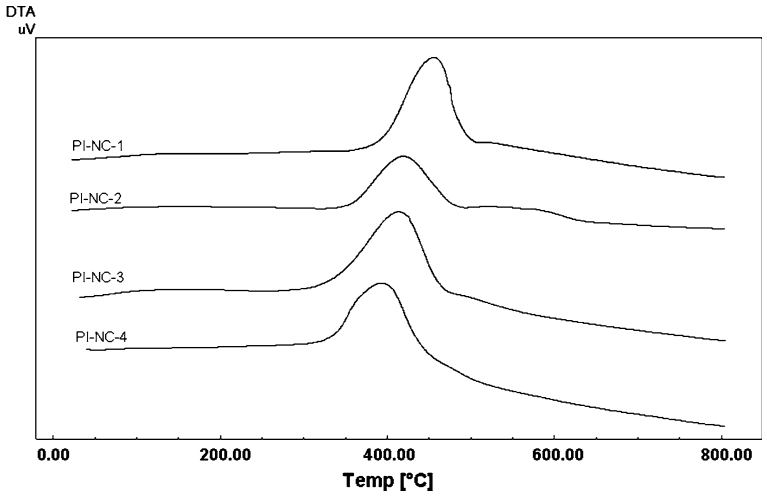

Fig. 5 DTA curves of PI–Fe_3O_4 nanocomposites

read in the subsequent heating DSC traces. The T_g values of polyimides (PI-NC-1–4) were in the 179–223 °C range depending on the structure of the dianhyride component and decreasing with increasing flexibility of the polymer backbones. As expected, the polyimide P1a derived from PMDA exhibited the highest T_g because of the rigid pyromellitimide unit. The thermal stability of the polymers was evaluated by TGA conducted at a heating rate of 10 °C/min in nitrogen atmosphere. The temperatures of 10% weight loss in nitrogen stayed within 395–419 °C range. PI-NC-3 having oxygen group in dianhyride exhibited the lowest T_{10} values than the other polyimides.

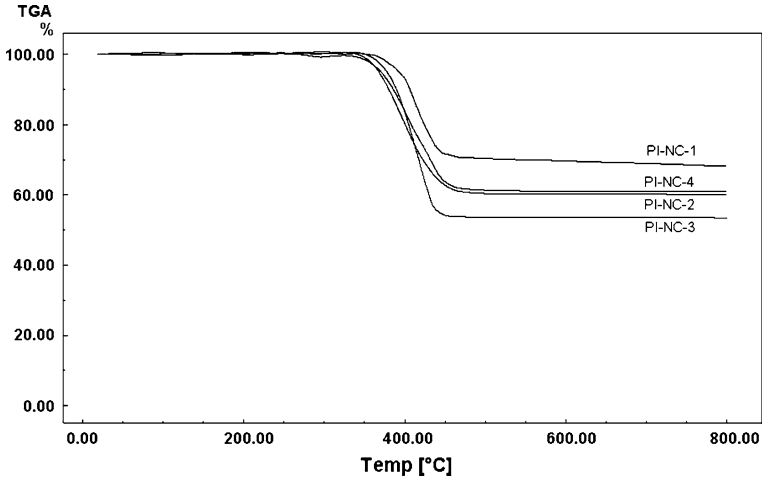

Fig. 6 TGA curves of PI–Fe_3O_4 nanocomposites

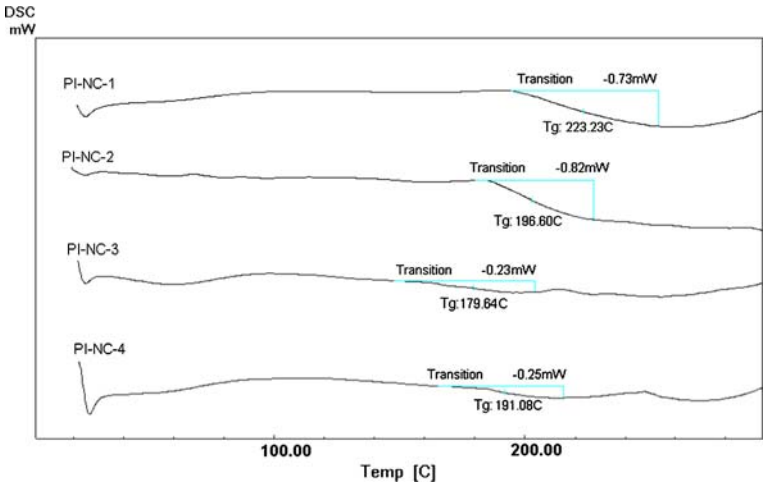

Fig. 7 DSC curves of PI–Fe_3O_4 nanocomposites

Energy-dispersive X-ray analysis (EDX) studies (Fig. 8) demonstrated that Fe_3O_4 nanoparticles seem to be dispersed randomly, although the particles do appear to form aggregates at increasing particle loadings. Iron oxide nanoparticles showed mosaic nanopatterns and nanoparticles surrounded by polyimides. The SEM image of PI–Fe_3O_4 shown as insert of Fig. 9 had uniform dispersion of the iron oxide particles in the polymer even covering the pores observed in the polyimide film. The films look more homogenous; however, particle agglomerates cannot be ruled out in this case also.

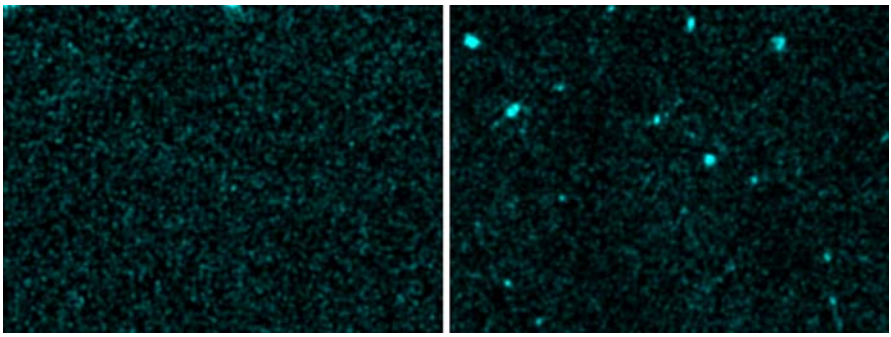

Fig. 8 EDX analysis of PI–Fe_3O_4 nanocomposites

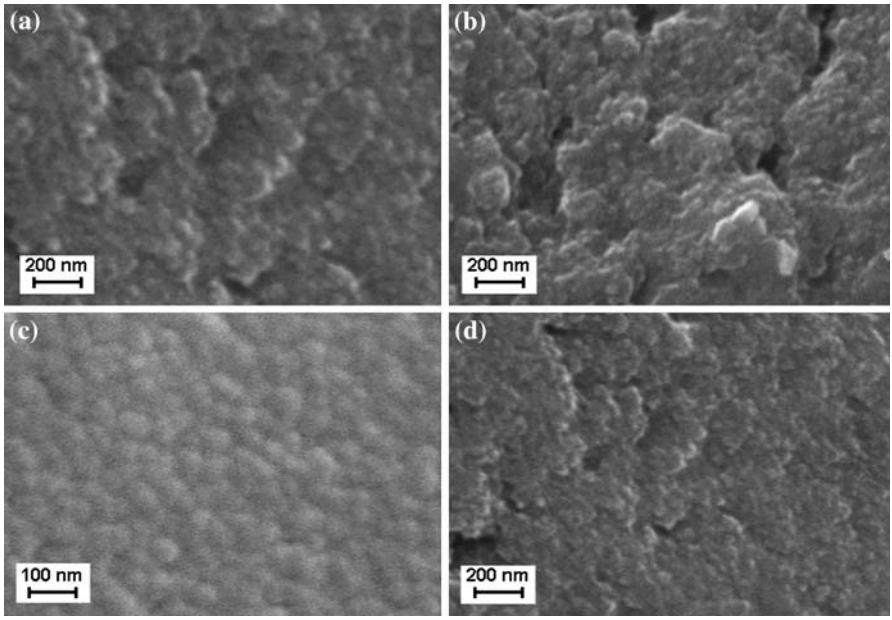

Fig. 9 SEM images of PI–Fe $_3O_4$ nanocomposites (**a** PI-NC-1, **b** PI-NC-2, **c** PI-NC-3, **d** PI-NC-4)

Magnetic hysteresis study

Figure 10 show the magnetic hysteresis loop at room temperature for APTS-coated Fe_3O_4 and PI–Fe_3O_4 nanocomposite (PI-NC-1). Magnetization measurements (magnetic hysteresis traces) have shown very high values of coercive force indicating their possible use in memory devices and in other related applications. The magnetic hysteresis results were interesting and also collaborate with the SEM images. On the basis of the magnetic hysteresis traces, we may conclude that the polymer matrix has hindered the free rotation of the easy axis of magnetization of Fe_3O_4 particles in the composite film.

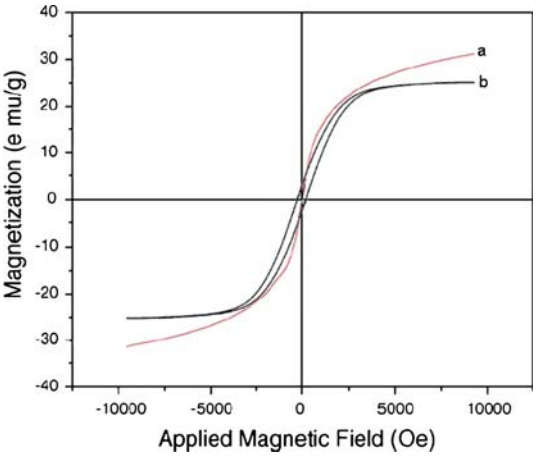

Fig. 10 Magnetic hysteresis loop trace of APTS-coated Fe_3O_4 (**a**) and PI–Fe_3O_4 nanocomposite (PI-NC-1) (**b**)

Conclusions

APTS-coated Fe_3O_4 can serve as a nanobuilding block for the preparation of polyimide hybrid materials. We described herein the synthesis of novel polyimides possessing Fe_3O_4 moieties in which the structure of the amino precursor contains an aliphatic CH_2 unit and the corresponding dianhyrides using two-stage polycondensation. The prepared polyimide–Fe_3O_4 nanocomposite films were characterized for their structure, morphology, and thermal behavior employing FTIR, SEM, transmission electron micrograph (TEM), XRD, 13C-NMR, and thermal analysis (DTA/TGA/DSC) techniques. Magnetic properties of polyimide–Fe_3O_4 nanocomposite, measured at room temperature by VSM. The strong interaction between Fe_3O_4 nanoparticles and polyimide matrix brings obvious effect on the thermal transition behavior and magnetic properties of composites. To improve the properties of composites, it is important to control the nanophase uniform dispersion in polymer matrix as well as the interaction of different hybrid components.

References

1. Ghosh MK, Mittal KL (eds) (1996) Polyimides: fundamentals and applications. Marcel Dekker, New York
2. Mittal KL (1984) Polyimides: synthesis, characterization, and applications. Plenum Press, New York
3. Abadie JM, Sillion B (eds) (1991) Polyimides and other high-temperature polymers. Elsevier, New York
4. Wilson D, Stenzenberger HD, Hergenrother PM (eds) (1990) Polyimides. Blackie, New York
5. Microyannidis JA (1997) Soluble and fusible polyamides and polyimides containing pyrazoline moieties and their crosslinking to heat-resistant resins. J Polym Sci A 35:1353
6. Woo Y, Oh SY, Kang YS, Jung B (2003) Synthesis and characterization of sulfonated polyimide membranes for direct methanol fuel cell. J Membr Sci 220:31
7. Yang CP, Hsiao SH, Hsu MF (2002) Organosoluble and light-colored fluorinated polyimides from 4,4′-bis(4-amino-2-trifluoromethylphenoxy)biphenyl and aromatic dianhydrides. J Polym Sci Part A Polym Chem 40:524

8. Reddy DS, Shu CF, Wu FI (2002) Synthesis and characterization of soluble polyimides derived from 2,2′-bis(3,4-dicarboxyphenoxy)-9,9′-spirobifluorene dianhydride. J Polym Sci Part A Polym Chem 40:262
9. Xie W, Heltsley R, Cai X, Deng F, Liu J, Lee C, Pan W-P (2002) Study of stability of high-temperature polyimides using TG/MS technique. J Appl Polym Sci 83:1219
10. Huang W, Yan D, Lu Q, Tao P (2002) Preparation of aromatic polyimides highly soluble in conventional solvents. J Polym Sci Part A Polym Chem 40:229
11. Yang CP, Hsiao S-H, Chen RS, Wei CS (2002) Chemical modification of 3,3′,4,4′-biphenyltetracarboxylic dianhydride polyimides by a catechol-derived bis(ether amine). J Appl Polym Sci 84:351
12. Han M, Nikles DE (2001) Amine-quinone polyimides. J Polym Sci Part A Polym Chem 39:4044
13. Yang CP, Chen RS, Yu CW (2001) Preparation and characterization of organosoluble polyimides based on 1,1-bis[4-(3,4aminophenoxy)phenyl]cyclohexane and commercial aromatic dianhydrides. J Appl Polym Sci 82:2750
14. Park JH, Jung JC, Sohn BH, Lee SW, Ree M (2001) Synthesis and characterization of novel polyimides containing stilbene unit in the side chain and their controllability of nematic liquid crystal alignment on the rubbed surfaces. J Polym Sci Part A Polym Chem 39:3622
15. Xu J, He C, Chung TS (2001) Synthesis and characterization of soluble polyimides derived from [1,1′;4′,1″]terphenyl-2′,5′-diol and biphenyl-2,5-diol. J Poly Sci Part A Polym Chem 39:2998
16. Xie K, Zhang SY, Liu JG, He MH, Yang SY (2001) Synthesis and characterization of soluble fluorine-containing polyimides based on 1,4-bis(4-amino-2-trifluoromethylphenoxy)benzene. J Polym Sci Part A Polym Chem 39:2581
17. Tong YJ, Huang XD, Chung TS (2001) A new strategy to prepare rodlike/flexible polyimide blends through poly(amic acid) amine salt precursors. Macromolecules 34:5748
18. Kim YS, Jung JC (2000) Synthesis and characterization of polyimides from 9,10-dialkyloxy-1,2,3,4,5,6,7,8-octahydro-2,3,6,7-anthracenetetracarboxylic-2,3:6,7-dianhydrides and 4,4′-oxydianiline. Polym Bull 45:11
19. Seckin T, Koytepe S, Cetinkaya B, Ozdemir I, Yigit B (2003) Synthesis and properties of novel polyimides from dichloro (1,3-p-dimethylaminobenzylimidazolidine-2-ylidene) p-cymene ruthenium (II). Des Monomers Polym 6:175
20. Seckin T, Cetinkaya E, Koytepe S, Yigit B (2003) Synthesis and properties of polyimides from 1,3-di(p-dimethylaminobenzyl)-imidazolidine-2-thion. Polym Bull 50:139
21. Seckin T, Köytepe S, Özdemir İ, Çetinkaya B, Demir S (2003) Novel type of metal-containing polyimides for the Heck and Suzuki–Miyaura cross-coupling reactions as highly active catalysts. J Inorg Organomet Polym 13:223
22. Gangopadhyay R, De A (2000) Conducting polymer nanocomposites: a brief overview. Chem Mater 12:608
23. Nalwa HS (2003) Handbook of organic–inorganic hybrid materials and nanocomposites. In: Gangopadhyay R, De A (eds) H-conducting polymer nanocomposites. American Scientific Publishers, California
24. Roucoux A, Schulz J, Patin H (2002) Reduced transition metal colloids: a novel family of reusable catalysts? Chem Rev 102:3757–3778
25. Heerbeek RV, Kamer PCJ, van Leeuwen PWNM, Reek JNH (2002) Dendrimers as support for recoverable catalysts and reagents. Chem Rev 102:3717–3756
26. Yeung LK, Crooks RM (2001) Heck heterocoupling within a dendritic nanoreactor. Nano Lett 1:14–17
27. Johnson BFG (1999) From clusters to nanoparticles and catalysis. Coord Chem Rev 190–192:1269–1285